[Article] DOI: 10.13208/j.electrochem.220205 Http://electrochem.xmu.edu.cn

Quantitative Lithium Composite as 3D Lithium Foam Anode for Lithium Metal Battery

Hu-Dong Li, Wei-Shang Jia*, Xin-Xiu Yan, Yao-Yue Yang*
(*Key Laboratory of General Chemistry of the National Ethnic Affairs Commission, School of Chemistry and Environment, Southwest Minzu University, Chengdu 610225, China*)

Abstract: Lithium (Li) metal as an anode material for batteries has extremely high specific capacity and extremely low redox potential, which can significantly improve the energy density of the battery. However, the main problems faced by the use of Li metal anodes are Li dendrite growth, interfacial side reaction and volumetric change of electrode. Herein, a strategy to prepare the three-dimensional (3D) Li foam by combining 3D scaffold with quantitative Li was proposed to suppress Li dendrites growth and alleviate electrode volumetric change. The 3D Li foam facilitated the efficient utilization of Li metal by suppressing the Li dendrite growth, mitigating the volumetric change, and improving the rate performance. Therefore, the cycling lifetime and rate performance of the symmetric cells using the 3D Li foam were improved. The EIS results showed that the 3D Li foam reduced the charge transfer resistance of the symmetric cells. And the average discharge specific capacity of the LTO cell during 1000 cycles was enhanced from 65 mAh·g^{-1} to 121 mAh·g^{-1} by using the 3D Li foam.

Key words: lithium metal anode; lithium dendrite; lithium foam; quantitative lithium composite electrode

1 Introduction

Portable electronic devices, storage power stations and electric vehicles have made considerable progress. At the same time, energy storage devices are also developing rapidly, and the market demands higher energy density and performance. Lithium (Li) ion batteries as the most matured and widely used electrochemical energy storage equipment also need to further improve their energy density to meet the needs of the market[1]. In the battery, the cathode and anode materials are very important to improve the overall energy density of the full battery. Therefore, cathode materials with higher voltage and specific capacity, and anode materials with lower voltage and higher specific capacity are continuously developed. Among them, Li metal anode is considered as the "holy grail" of Li batteries owing to its high specific capacity of 3860 mAh·g^{-1} and low redox potential of -3.04 V vs. standard hydrogen electrode (SHE), which can greatly increase the energy density of Li batteries[2-6]. This also aroused great enthusiasm of extensive researchers[7,8].

However, there are three major problems of Li metal anodes, including Li dendrite growth, interfacial parasitic reaction, and large volumetric change, which restrict their practical application[9-13]. In order to solve the problems of Li dendrite and interface instability, interfacial modification[14,15], electrolyte additives[16,17] and novel electrolyte[18] can be used to suppress Li dendrite growth and alleviate interface side reaction.

Cite as: Li H D, Jia W S, Yan X X, Yang Y Y. Quantitative lithium composite as 3D lithium foam anode for lithium metal battery. *J. Electrochem.*, 2022, 28(8): 2202051.

Received: 2022-02-07, Revised: 2022-03-02. *Corresponding author, Tel: (86) 18109081657, E-mail: jiaweishang@swun.edu.cn (W. S. Jia); Tel: (86-28)85709707, yaoyueyoung@swun.edu.cn (Y. Y. Yang)

Nevertheless, to reduce the volumetric change of Li anode during charge and discharge processes, it is necessary to design and introduce 3D current collector, including Cu foam, Ni foam, graphene, carbon nanotubes, etc[19-23]. The 3D scaffold can inhibit Li dendrite growth by reducing the actual current density and providing the space of Li deposition. Furthermore, pre-storage of Li metal in 3D scaffold to form 3D composite Li metal anode is essential for full battery, especially for Li-free cathode materials. Thus, composite Li metal electrodes with different 3D scaffolds have been developed and fabricated[24,25]. At present, the preparation method of composite Li metal electrode is mainly combination the 3D scaffold with molten Li and Li electroplating in the 3D scaffold. The method of combining 3D scaffold with molten Li is more conducive to a large-scale application[26,27]. However, the research on the combination of 3D scaffold and quantitative Li metal needs further systematic investigation[28].

In this work, a strategy of 3D Li foam preparation by combining 3D scaffold with quantitative molten Li metal was proposed, which is suitable for any lithiophilic scaffold. The lithiophilic Cu foam was used as the scaffold to combine with quantitative molten Li, and taken as an example. It has been reported that Li metal and Cu metal formed an alloy at high temperature, indicating that molten Li metal could dissolve a certain amount of Cu metal, and form some nanowires spontaneously during the cooling process[29]. Therefore, the proposed method can form some finer structures on the surface of the Cu foam and increase the specific surface area of the Cu foam as a scaffold. 3D Li foam as an anode is conducive to efficient utilization of Li metal, thus, the 3D Li foam anode has a large contact area with the electrolyte, which can provide more reaction sites and improve the rate performance of the battery. Furthermore, the 3D Li foam can suppress Li dendrite growth and alleviate volumetric change by providing a larger specific surface area and more space of Li deposition than the planar Li foil. Hence, the symmetric cells with the 3D Li foam exhibit longer lifespan, smaller polarization and better rate performance. The performance of the LTO cell with the 3D Li foam is better than that of the planar Li foil.

2 Experimental Section

2.1 Fabrication of 3D Li Foam

The Cu foam with a thickness of 500 μm was purchased from Guangdong Canrd New Energy Technology Co., Ltd., and Li foil with a thickness of 175 μm was purchased from Chengdu Denway Newtype Metal Material Co., Ltd. The Cu foam was washed by deionized water and anhydrous ethanol three times, and then transferred to a glovebox after a vacuum oven drying. Preparation and storage of 3D Li foam were performed in an argon-filled glovebox with less than 0.1 ppm H_2O and 0.1 ppm O_2. The Cu foam was punched into a disc of ~ 15 mm in diameter and ~ 112 mg in weight. Quantitative Li wafer of 17 mg in weight and 15 mm in diameter was stacked on a Cu foam and heated to 420 °C on a hot plate (IKA C-MAG HP4). The Cu foam was soaked with molten Li through capillary action and formed a 3D scaffold wrapped with Li metal, and then 3D Li foam was obtained after cooling to room temperature.

2.2 Preparation of LTO Electrode

The LTO powder and super P were fully ground in an agate mortar, and added to poly(vinyl difluoride) (PVDF) solution with N-Methyl-2-pyrrolidone (NMP) as the solvent, and the mass ratio of LTO powder:super P:PVDF was 8:1:1. The mixture was further ground to form a uniform slurry, and then coated on Cu foil by a scraper. After drying in an oven at 120 °C for 12 h, the LTO electrode was punched into a disc of 12 mm in diameter. The areal mass loading of LTO electrode was about 2 $mg \cdot cm^{-2}$.

2.3 Cell Assembly

CR2032 type coin cells were used for cell assembly. For symmetric cells, the planar Li foil or the 3D Li foam was used as the working electrode and counter electrode, and Celgard 2325 was used as the separator. The employed electrolyte was 1.0 $mol \cdot L^{-1}$ lithium bis(trifluoromethanesulphonyl)imide (LiTFSI) in a mixture of 1,3-dioxolane (DOL) and 1,2-dimethoxyethane (DME) (1:1 by *v*/*v*) with 2wt% lithium ni-

trate ($LiNO_3$) as an additive. For LTO cells, the LTO electrode, planar Li foil or 3D Li foam and Celgard 2325 were used as the working electrode, counter electrode and separator, respectively. The employed electrolyte was 1.0 mol·L^{-1} lithium hexafluorophosphate ($LiPF_6$) in a mixture of ethylene carbonate (EC), diethyl carbonate (DEC) and dimethyl carbonate (DMC) (1:1:1 by *v*/*v*/*v*) with 5wt% fluoroethylene carbonate (FEC) as an additive.

2.4 Electrochemical Measurements and Characterization

The cell galvanostatic cycling tests were conducted on a multichannel battery test system (CT-4008, Neware Battery Testing System). The EIS measurements were tested on an electrochemical workstation (CHI 660E, Shanghai Chenhua Instrument Co., Ltd.) and recorded over the frequency range of 100 kHz to 0.1 Hz with an amplitude of 5 mV.

The Li foam and Li foil after cycling for further characterization were obtained from the disassembled cells, and then rinsed by DME to remove residual electrolyte. The obtained samples were dried under vacuum. The morphologies of Li foam and Li foil before and after cycling were observed by a field-emission scanning electron microscope (FE-SEM, FEI Inspect F, 20 kV). The samples were sealed in an argon-filled airtight container and transferred to the SEM system immediately. The X-ray diffraction (XRD) tests were carried out on an Empyrean with Cu K_α irradiation (λ = 1.5418 Å, tube voltage: 40 kV and tube current: 35 mA). The sample for XRD testing was coated by a layer of polyimide tape to protect it from air.

3 Results and Discussion

3.1 Microstructure of 3D Li Foam

Firstly, the microstructure of 3D Li foam was observed by SEM and analyzed. The thickness of Cu foam was about 500 μm with the pore size of about 200 μm. The microscopic morphologic images and digital photographs of the Cu foam, Li foam and Li foam after stripping are shown in Figure 1(b-j). The microscopic surface of the Cu foam appeared relatively smooth. However, after the combination of Cu foam with a quantitative molten Li, the color of the formed 3D Li foam became yellow, and its microscopic morphology was changed. The surface of the scaffold of Cu foam was covered with a layer of metallic Li, and the surface of the scaffold became granular with a larger specific surface area, which is beneficial to increase the specific surface area of Cu foam and improve the electrochemical performance of 3D current collector, because molten Li reacts with Cu foam to form Li-Cu alloy as reported previously[29-31]. After the complete electrochemical stripping, the Cu foam still maintained a complete 3D scaffold structure and a granular surface.

According to Sand's law, growth of Li dendrites starts at time (τ) that follows a power law as a function of current density[32,33].

$$\tau \sim \pi D\left(\frac{eC_0}{2J}\right)^2\left(\frac{\mu_a+\mu_c}{\mu_a}\right)^2 \quad (1)$$

where D is the ambipolar diffusion coefficient, e is the electronic charge, C_0 is the electrolyte concentration in bulk solution, μ_a and μ_c are the anionic and cationic mobilities, respectively, and J is the practical current density at the Li surface. Apparently, the growth of Li dendrites could be delayed by reducing practical current density. Herein, the 3D Li foam can reduce practical current density by increasing specific surface area of conductive current collector and accommodate the volumetric change by providing space for Li plating during the charge/discharge process[34].

3.2 Structural and Surface Analyses

In order to investigate the change of scaffold structure during the synthesis of Li foam, the XRD tests of Li foil, Li foil after cycling, Cu foil, Li foam and Li foam after cycling were carried out. As depicted in Figure 2(a), the XRD patterns of planar Li foil before and after cycling demonstrated that the crystal structure of planar Li foil did not change much after 10 cycles. Compared with the Cu foam, each characteristic diffraction peak of Cu crystals on the Li foam was split into two peaks, and there was one more peak shifted to a low angle. According to the Bragg equation, a low angle shift in diffraction peak of the crystals to indicates larger lattice size . In this case, it

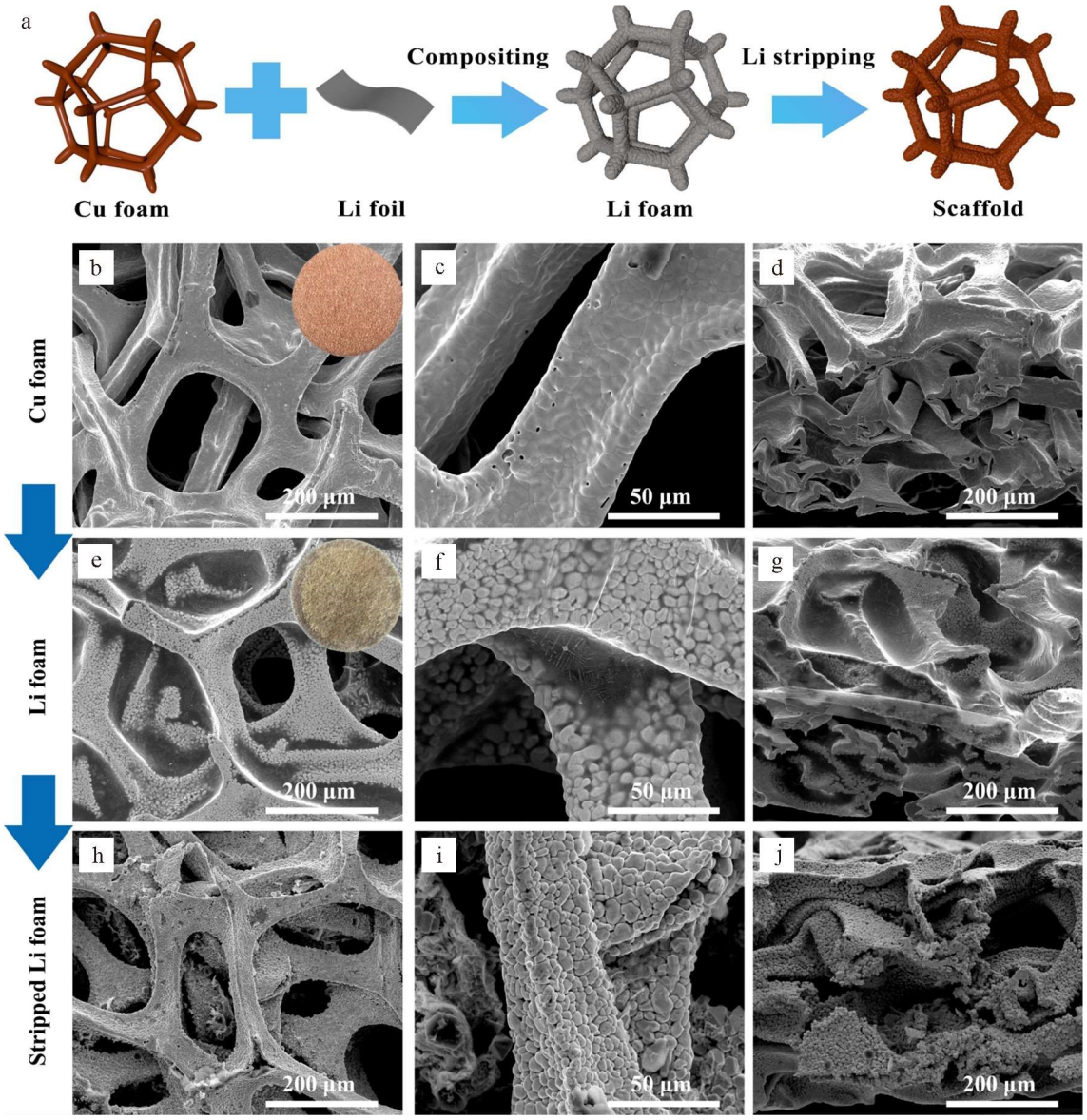

Figure 1 Schematic illustration showing the preparation process of 3D Li foam (a); SEM images of Cu foam (b-d); 3D Li foam (e-g); 3D Li foam after complete stripping (h-j). The insets in (b) and (e) are the photos of Cu and Li foams, respectively. (color on line)

may be caused by the entry of Li atoms into the Cu lattice to form a substitutional solid solution[29]. Thus, the Li foam contained three components, Li metal, Cu metal and Li-Cu solid solution. The structure of the Li-Cu solid solution did not change after 10 cycles, suggesting that the Li-Cu solid solution structure remained stable during the Li stripping and plating. However, the metallic Li in the Li foam did not show strong characteristic peaks. Only one weak diffraction peak appeared, belonged to the (110) crystal plane. This may be because the Cu foam affected the crystallization behavior of Li metal and changed the crystal structure of Li metal in the process of combination with Cu foam. Besides, all the XRD patterns showed an amorphous broad peak at about 18 degrees. This is caused by the polyimide tape coated on the surface of the test sample, which was used to protect the sample from air.

In order to study the electrochemical stripping behavior of Li foam and its microscopic morphology after stripping, the complete stripping of Li foam was carried out. And the discharge curve is shown in

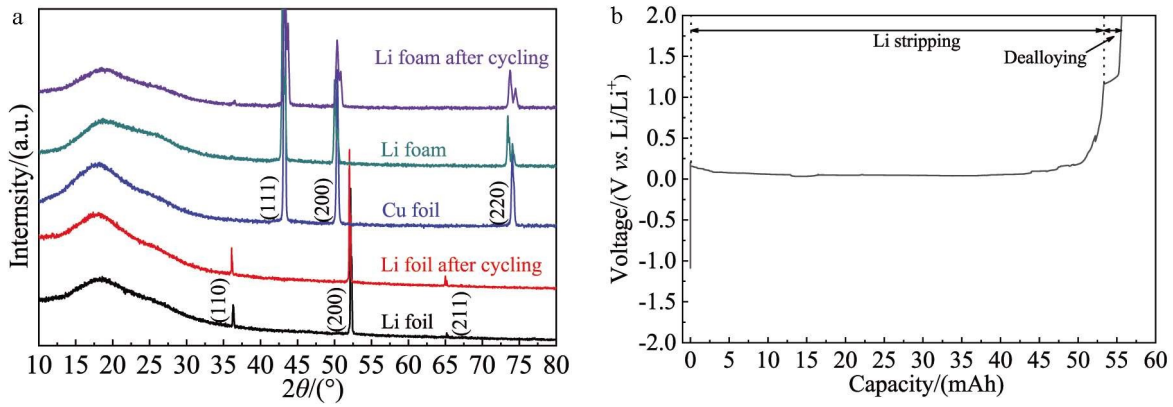

Figure 2 XRD patterns of the 3D Li foam and planar Li foil before and after cycling (a); discharge curves of the 3D Li foam (b). (color on line)

Figure 2(b). The capacity of Li stripping was about 55.6 mAh, which is close to the theoretical capacity of quantitative Li metal (17 mg, 65.6 mAh). According to the mass of Cu foam being about 112 mg, the theoretical specific capacity of Li foam is calculated to be about 585.7 mAh·g^{-1}, and the actual specific capacity is about 496.4 mAh·g^{-1}. The loss capacity of Li mainly came from the formation of Li-Cu solid solution alloy and the residual Li metal during stripping. There were two plateaus in the discharge process, corresponding to the Li stripping (-0.045 V) and the dealloy of Li-Cu alloy (-1.2 V). Besides, the analyses of chemical compositions on the surfaces of 3D Li foam and planar Li foil after cycling were conducted by XPS. As shown in Figure 3, the obtained F1s, N1s, C1s, O1s and S2p spectra on the surfaces of the 3D Li foam and planar Li foil after cycling were very similar. But the peak positions in the Li1s spectra of 3D Li foam and planar Li foil were different, which may be due to the influence of Li-Cu alloy. This result is consistent with the weakening of the characteristic peak of Li metal in the XRD data of the Li foam.

3.3 Li Stripping and Plating Behaviors

The Li stripping and plating behaviors of the 3D Li foam and planar Li foil were investigated by SEM to verify the effects of suppressing Li dendrites and alleviating electrode volumetric change of Li foam. The micromorphologies of the Li stripping and plating of Li foam are shown in Figure 4. As the capacity of Li stripping increased, the scaffold structure of the Cu foam was gradually revealed, and the granular morphology on the Cu foam surface formed by the alloying could be clearly seen. The cross-sectional SEM images of the 3D Li foam show that as the Li was stripped from top to bottom, the scaffold structure remained unchanged, which can maintain the stability of the electrode structure. When the Li plating started, Li began to be deposited from the scaffold structure and gradually grew, the surface morphology of Li foam was relatively smooth, and the Li deposition inside the scaffold appeared dendrite-like. But the 3D scaffold could accommodate Li dendrites to avoid Li dendrites upward growing through the porous separator. Thanks to the effect of the 3D scaffold, the volume of the electrode did not change significantly after the Li deposition from the cross-sectional view.

On the contrary, the volume and structure of the planar Li foil changed significantly during the Li stripping and plating processes. As depicted in Figure 5, when the Li stripping started, corrosion-like pits appeared on the surface of the planar Li foil. These pits were not uniformly distributed on the surface of the planar Li foil, and some areas were more, while some areas were less. With the increase of the Li stripping capacity, the pits on the Li surface became more, larger and deeper. From the cross-sectional SEM images in Figure 5, the planar Li foil was get-

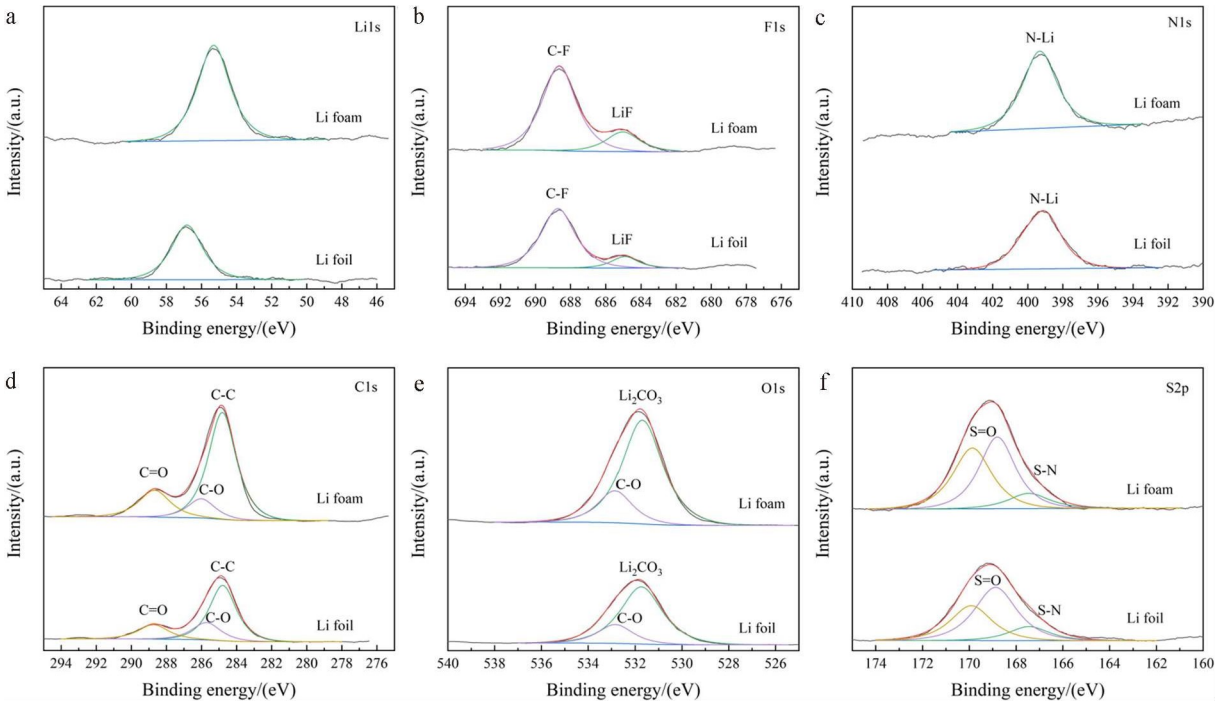

Figure 3 XPS fine spectra of Li1s (a), F1s (b), N1s (c), C1s (d), O1s (e), and S2p (f) for the Li foam and Li foil. (color on line)

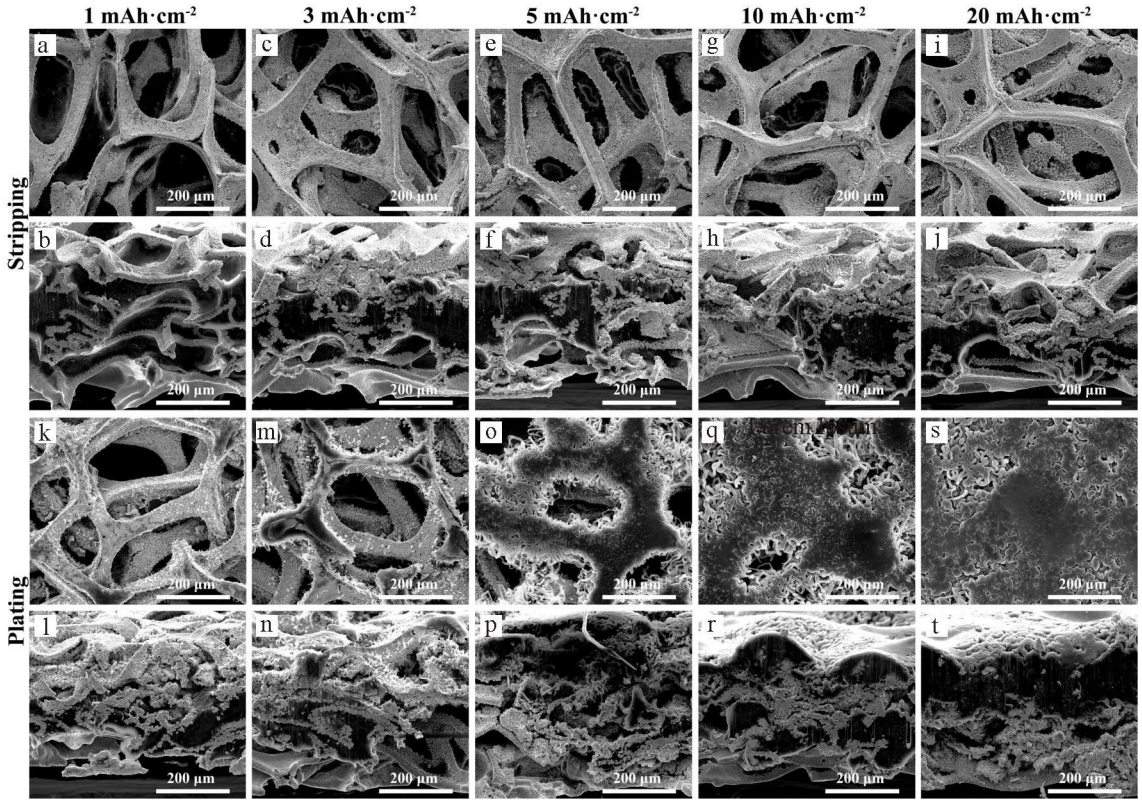

Figure 4 Top-view and cross-sectional SEM micrographs of the 3D Li foam stripping on 1.0 mAh·cm^{-2} (a-b), 3.0 mAh·cm^{-2} (c-d), 5.0 mAh·cm^{-2} (e-f), 10.0 mAh·cm^{-2} (g-h), 20.0 mAh·cm^{-2} (i-j), and then plating on 1.0 mAh·cm^{-2} (k-l), 3.0 mAh·cm^{-2} (m-n), 5.0 mAh·cm^{-2} (o-p), 10.0 mAh·cm^{-2} (q-r), 20.0 mAh·cm^{-2} (s-t).

ting thinner and thinner. After the Li stripping on 20.0 mAh·cm^{-2}, the Li deposition began. Li would be preferentially deposited inside the pits. With the increase of the Li plating capacity, the planar Li foil became thicker. And Li was deposited on the surface of the Li foil to form a large number of Li dendrites, which increased the specific surface area and volume of the planar Li foil. Therefore, this result indicates that the Li foam can inhibit the growth of Li dendrites and alleviate the volumetric change of the electrode during Li stripping and plating processes.

3.4 Electrochemical Performances

To further investigate the effect of the Li foam on the electrochemical performance, symmetric cells were assembled for galvanostatic test. The result is shown in Figure 6. The cycling lifetime of the symmetric Li foam cell was more than 3000 h, while that of the symmetric Li foil cell was about 1000 h, when the current density was 1.0 mA·cm^{-2} and the areal charge/discharge capacity was 1.0 mAh·cm^{-2}. Furthermore, the 3D Li foam exhibited smaller polarization, which is consistent with the EIS results. Before cycling, the charge transfer impedance of the symmetric Li foam cell was about 190 Ω, while that of the symmetric Li foil cell was about 1250 Ω. After 10 cycles at 1.0 mA·cm^{-2}, the charge transfer resistances of both symmetric cells were reduced. The charge transfer resistance of the symmetric Li foam cell was still much smaller than that of the symmetric Li foil cell. When the current density increasd to 3.0 mA·cm^{-2}, the trend of performance was similar to that at 1.0 mA·cm^{-2}. The cycling lifetime of the symmetric Li foam cell was more than 800 h. While the polarization of the symmetric Li foil cell increased rapidly, and the voltage curve gradually showed fluctuations after 400 h. The rate performance test results also showed that the 3D Li foam performed better than the planar Li foil.

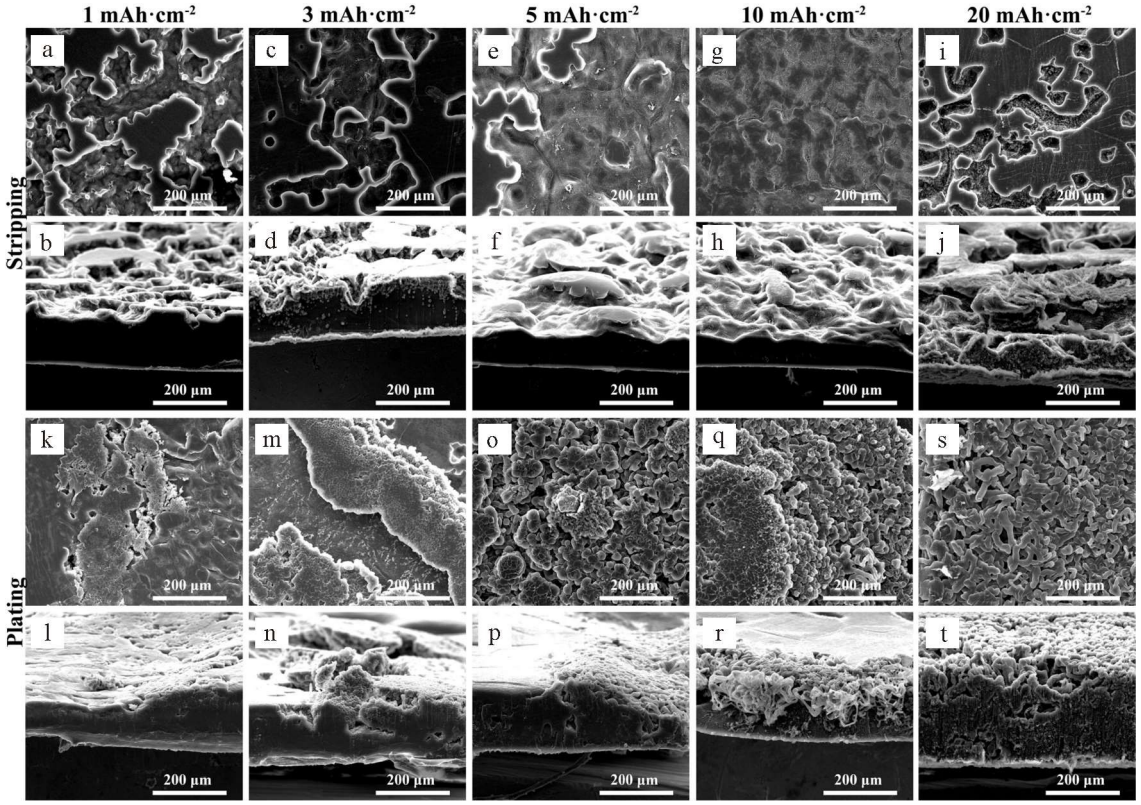

Figure 5 Top-view and cross-sectional SEM micrographs of the planar Li foil stripping on 1.0 mAh·cm^{-2} (a-b), 3.0 mAh·cm^{-2} (c-d), 5.0 mAh·cm^{-2} (e-f), 10.0 mAh·cm^{-2} (g-h), 20.0 mAh·cm^{-2} (i-j), and then plating on 1.0 mAh·cm^{-2} (k-l), 3.0 mAh·cm^{-2} (m-n), 5.0 mAh·cm^{-2} (o-p), 10.0 mAh·cm^{-2} (q-r), 20.0 mAh·cm^{-2} (s-t).

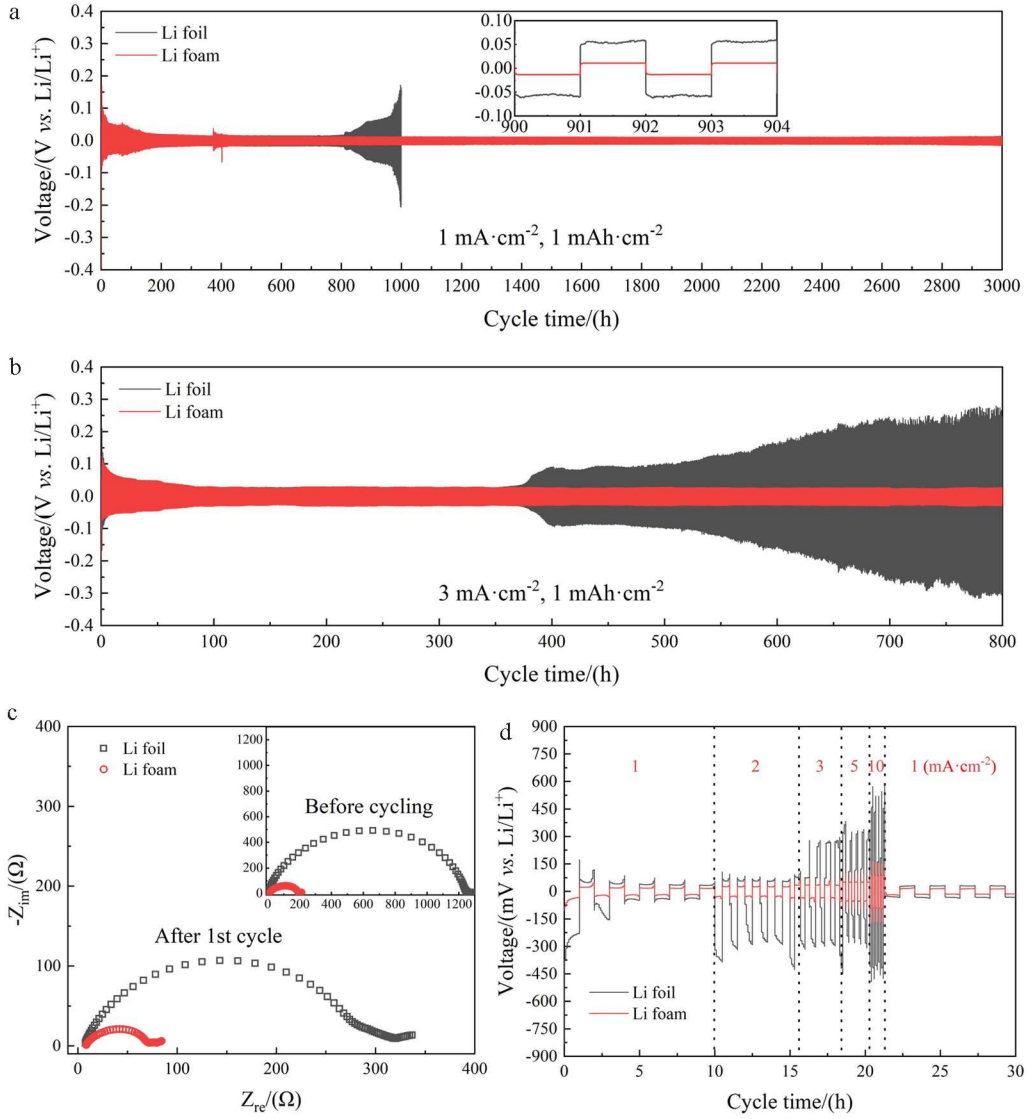

Figure 6 Voltage-time profiles of the symmetric cells using the 3D Li foam and planar Li foil at a current density of 1.0 mA·cm^{-2} (a) and 3.0 mA·cm^{-2} with the areal charge/discharge capacity of 1.0 mAh·cm^{-2}; Nyquist plots of the symmetric cells using the 3D Li foam and planar Li foil before and after cycling (c); Voltage-time profiles of the symmetric cell using the 3D Li foam and planar Li foil at different rates varying from 1.0 to 10.0 mA·cm^{-2} with the areal charge/discharge capacity of 1.0 mAh·cm^{-2} (d). (color on line)

Finally, a full cell was assembled to test the effect of the 3D Li foam. The results are given in Figure 7. The performance of the LTO cell using the 3D Li foam was improved compared to that using the planar Li foil, because the 3D Li foam could effectively suppress the growth of Li dendrite and its 3D structure was conducive to the improvement in the high rate performance of the battery. Consequently, the average discharge specific capacity of the LTO cell using the 3D Li foam during 1000 cycles was about 121 mAh·g^{-1}, while that using the planar Li foil was about 65 mAh·g^{-1}.

4 Conclusions

In summary, a strategy of the 3D Li foam preparation by combining lithiophilic 3D scaffold with quantitative Li metal was proposed. The quantitative Li was heated to form molten Li, which could quickly infiltrate the surface of the lithiophilic 3D scaffold to form porous 3D Li foam. The 3D Li foam could suppress the growth of Li dendrite, alleviate the volumetric change and improve the rate performance during the Li stripping and plating processes. Compared

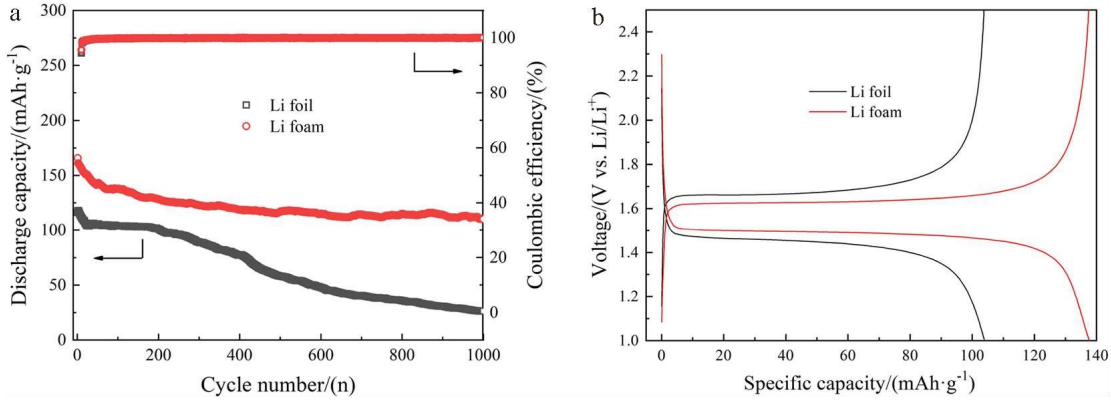

Figure 7 Cycling performance curves of the LTO cells using the 3D Li foam and planar Li foil at 5 C rate (a) and the charge and discharge curves at the 100th cycle (b). (color on line)

with the planar Li foil, the 3D Li foam became more conducive to the efficient use of Li metal anode. As a result, the electrochemical performances of the symmetric cells were improved by using the 3D Li foam, including the increased cycling lifetime, the reduced polarization and the improved rate performance. The LTO cell using the 3D Li foam also exhibited better cycling performance and stability.

Acknowledgements:

This work is supported by the National Natural Science Foundation of China (No. 22172121), and the Southwest Minzu University Innovation Project for Graduate Students (No. CX2021SZ08).

References:

[1] Scrosati B, Hassoun J, Sun Y K. Lithium-ion batteries. A look into the future[J]. Energy Environ. Sci., 2011, 4(9): 3287-3295.

[2] Chu S, Cui Y, Liu N. The path towards sustainable energy [J]. Nat. Mater., 2017, 16(1): 16-22.

[3] Xu W, Wang J L, Ding F, Chen X L, Nasybulin E, Zhang Y H, Zhang J G. Lithium metal anodes for rechargeable batteries[J]. Energy Environ. Sci., 2014, 7(2): 513-537.

[4] Lin D C, Liu Y Y, Cui Y. Reviving the lithium metal anode for high-energy batteries[J]. Nat. Nanotechnol., 2017, 12(3): 194-206.

[5] Choi J W, Aurbach D. Promise and reality of post-lithium-ion batteries with high energy densities[J]. Nat. Rev. Mater., 2016, 1(4): 16013.

[6] Goodenough J B, Kim Y. Challenges for rechargeable Li batteries[J]. Chem. Mater., 2010, 22(3): 587-603.

[7] Wang D, Liu Y M, Li G W, Qin C C, Huang L, Wu Y P. Liquid metal welding to suppress Li dendrite by equalized heat distribution[J]. Adv. Funct. Mater., 2021, 31(47): 2106740.

[8] Wang D, Qin C C, Li X L, Song G Q, Liu Y M, Cao M Y, Huang L, Wu Y P. Synchronous healing of Li metal anode via asymmetrical bidirectional current[J]. iScience, 2020, 23(1): 100781.

[9] Lin D C, Liu Y Y, Pei A, Cui Y. Nanoscale perspective: materials designs and understandings in lithium metal anodes[J]. Nano Res., 2017, 10(12): 4003-4026.

[10] Kong L, Peng H J, Huang J Q, Zhang Q. Review of nanostructured current collectors in lithium-sulfur batteries[J]. Nano Res., 2017, 10(12): 4027-4054.

[11] Shi S Q, Gao J, Liu Y, Zhao Y, Wu Q, Ju W W, Ouyang C Y, Xiao R J. Multi-scale computation methods: Their applications in lithium-ion battery research and development[J]. Chinese Phys. B, 2016, 25(1): 018212.

[12] Liu F, Xu R, Wu Y C, Boyle D T, Yang A K, Xu J W, Zhu Y Y, Ye Y S, Yu Z A, Zhang Z W, Xiao X, Huang W X, Wang H S, Chen H, Cui Y. Dynamic spatial progression of isolated lithium during battery operations[J]. Nature, 2021, 600(7890): 659-663.

[13] Zhang Z W, Li Y Z, Xu R, Zhou W J, Li Y B, Oyakhire S T, Wu Y C, Xu J W, Wang H S, Yu Z A, Boyle D T, Huang W, Ye Y S, Chen H, Wan J Y, Bao Z N, Chiu W, Cui Y. Capturing the swelling of solid-electrolyte interphase in lithium metal batteries[J]. Science, 2022, 375 (6576): 66-70.

[14] Jia W S, Wang Q J, Yang J Y, Fan C, Wang L P, Li J Z. Pretreatment of lithium surface by using iodic acid (HIO_3) to improve its anode performance in lithium batteries[J]. ACS Appl. Mater. Inter., 2017, 9(8): 7068-7074.

[15] Luo Z, Qiu X J, Liu C, Li S, Wang C W, Zou G Q, Hou

H S, Ji X B. Interfacial challenges towards stable Li metal anode[J]. Nano Energy, 2021, 79: 105507.

[16] Jia W S, Fan C, Wang L P, Wang Q J, Zhao M J, Zhou A J, Li J Z. Extremely accessible potassium nitrate (KNO_3) as the highly efficient electrolyte additive in lithium battery[J]. ACS Appl. Mater. Inter., 2016, 8(24): 15399-15405.

[17] Zheng J M, Engelhard M H, Mei D H, Jiao S H, Polzin B J, Zhang J G, Xu W. Electrolyte additive enabled fast charging and stable cycling lithium metal batteries [J]. Nat. Energy, 2017, 2(3): 17012.

[18] Jiao S H, Ren X D, Cao R G, Engelhard M H, Liu Y Z, Hu D H, Mei D H, Zheng J M, Zhao W G, Li Q Y, Liu N, Adams B D, Ma C, Liu J, Zhang J G, Xu W. Stable cycling of high-voltage lithium metal batteries in ether electrolytes[J]. Nat. Energy, 2018, 3(9): 739-746.

[19] Xiang J W, Yuan L X, Shen Y, Cheng Z X, Yuan K, Guo Z Z, Zhang Y, Chen X, Huang Y H. Improved rechargeability of lithium metal anode via controlling lithium-ion flux[J]. Adv. Energy Mater., 2018, 8(36): 1802352.

[20] Zhang R, Cheng X B, Zhao C Z, Peng H J, Shi J L, Huang J Q, Wang J F, Wei F, Zhang Q. Conductive nanostructured scaffolds render low local current density to inhibit lithium dendrite growth[J]. Adv. Mater., 2016, 28(11): 2155-2162.

[21] Zhang R H, Li Y, Qiao L, Li D W, Deng J L, Zhou J J, Xie L, Hou Y, Wang T, Tian W, Cao J C, Cheng F L, Yang B, Liang K, Chen P, Kong B. Atomic layer deposition assisted superassembly of ultrathin ZnO layer decorated hierarchical Cu foam for stable lithium metal anode [J]. Energy Storage Mater., 2021, 37: 123-134.

[22] Ye H, Xin S, Yin Y X, Li J Y, Guo Y G, Wan L J. Stable Li plating/stripping electrochemistry realized by a hybrid Li reservoir in spherical carbon granules with 3D conducting skeletons[J]. J. Am. Chem. Soc., 2017, 139(16): 5916-5922.

[23] Jia W S, Chen T, Wang Y, Qu S J, Yao Z Y, Liu Y C, Yin Y, Zou W, Zhou F, Li J Z. Porous equipotential body with heterogeneous nucleation sites: A novel 3D composite current collector for lithium metal anode[J]. Electrochim. Acta, 2019, 309: 460-468.

[24] Shi P, Zhang X Q, Shen X, Zhang R, Liu H, Zhang Q. A review of composite lithium metal anode for practical applications[J]. Adv. Mater. Technol., 2020, 5(1): 1900806.

[25] Wang H S, Liu Y Y, Li Y Z, Cui Y. Lithium metal anode materials design: Interphase and host[J]. Electrochem. Energy Rev., 2019, 2(4): 509-517.

[26] Hafez A M, Jiao Y C, Shi J J, Ma Y, Cao D X, Liu Y Y, Zhu H L. Stable metal anode enabled by porous lithium foam with superior ion accessibility[J]. Adv. Mater., 2018, 30(30): 1802156.

[27] Huang S B, Chen L, Wang T S, Hu J K, Zhang Q F, Zhang H, Nan C W, Fan L Z. Self-propagating enabling high lithium metal utilization ratio composite anodes for lithium metal batteries[J]. Nano Lett., 2021, 21(1): 791-797.

[28] Yang T Z, Sun Y W, Qian T, Liu J, Liu X J, Rosei F, Yan C L. Lithium dendrite inhibition via 3D porous lithium metal anode accompanied by inherent SEI layer[J]. Energy Storage Mater., 2020, 26: 385-390.

[29] Jia W S, Liu Y C, Wang Z H, Qing F Z, Li J Z, Wang Y, Xiao R J, Zhou A J, Li G B, Yu X Q, Hu Y S, Li H, Wang Z X, Huang X J, Chen L Q. Low-temperature fusion fabrication of Li-Cu alloy anode with *in situ* formed 3D framework of inert $LiCu_x$ nanowires for excellent Li storage performance[J]. Sci. Bull., 2020, 65(22): 1907-1915.

[30] Jia W S, Li H D, Wang Z H, Liu Y C, Yang Y Y, Li J Z. 3D composite lithium metal with multilevel micro-nano structure combined with surface modification for stable lithium metal anodes[J]. Appl. Surf. Sci., 2021, 570: 151159.

[31] Adair K R, Iqbal M, Wang C H, Zhao Y, Banis M N, Li R Y, Zhang L, Yang R, Lu S G, Sun X L. Towards high performance Li metal batteries: Nanoscale surface modification of 3D metal hosts for pre-stored Li metal anodes [J]. Nano Energy, 2018, 54: 375-382.

[32] Chazalviel J N. Electrochemical aspects of the generation of ramified metallic electrodeposits[J]. Phys. Rev. A, 1990, 42(12): 7355-7367.

[33] Jin S, Sun Z W, Guo Y L, Qi Z K, Guo C K, Kong X H, Zhu Y W, Ji H X. High areal capacity and lithium utilization in anodes made of covalently connected graphite microtubes[J]. Adv. Mater., 2017, 29(38): 1700783.

[34] Zuo T T, Wu X W, Yang C P, Yin Y X, Ye H, Li N W, Guo Y G. Graphitized carbon fibers as multifunctional 3D current collectors for high areal capacity Li anodes[J]. Adv. Mater., 2017, 29(29): 1700389.

定量的复合金属锂作为三维泡沫锂电极用于锂电池的研究

李虎东,贾维尚*,闫新秀,阳耀月*

(西南民族大学化学与环境学院,化学基础国家民委重点实验室,四川 成都 610225)

摘要: 金属锂作为电池的负极材料具有极高的比容量和极低的氧化还原电位,能够显著提升电池的能量密度。然而,金属锂负极在实际应用中所面临的主要问题是锂枝晶、界面副反应和电极体积变化大的难题。在本文中,我们提出了一种通过将定量的金属锂与三维骨架进行复合形成三维泡沫锂负极的策略, 并利用三维泡沫锂来抑制锂枝晶的生长和缓解电极的体积变化。因此,三维泡沫锂电极有利于金属锂负极的高效利用,并能借助其与平面锂箔相比更高的比表面积和更多的反应位点来提升电池的倍率性能。因此,通过采用三维泡沫锂,对称电池的循环寿命和倍率性能都得到了有效的提升。EIS 数据结果表明,三维泡沫锂能够减小对称电池的电荷转移阻抗。而且,将三维泡沫锂作为负极组装的 LTO 全电池,与锂箔作为负极相比,循环 1000 周平均放电比容量从 65 $mAh\cdot g^{-1}$ 提升至 121 $mAh\cdot g^{-1}$。

关键词: 金属锂负极;锂枝晶;泡沫锂;定量的锂复合电极